Cavitation dynamics and directional microbubble ejection induced by intense femtosecond laser pulses in liquids

Faccio, Daniele Franco Angelo; Tamosauskas, G.; Rubino, E.; Darginavicius, J.; Papazoglou, D. G.; Tzortzakis, S.; Couairon, A.; Dubietis, A.

Published in:
Physical Review E

DOI:
10.1103/PhysRevE.86.036304

Publication date:
2012

Cavitation dynamics and directional microbubble ejection induced by intense femtosecond laser pulses in liquids

D. Faccio,[1] G. Tamošauskas,[2] E. Rubino,[3] J. Darginavičius,[2] D. G. Papazoglou,[4,5] S. Tzortzakis,[4,5] A. Couairon,[6] and A. Dubietis[2]

[1]*School of Engineering and Physical Sciences, SUPA, Heriot-Watt University, Edinburgh EH14 4AS, Scotland, United Kingdom*
[2]*Department of Quantum Electronics, Vilnius University, Sauletekio Avenue 9, Building 3, LT-10222 Vilnius, Lithuania*
[3]*Dipartimento di Scienza e Alta Tecnologia, Università dell'Insubria, Via Valleggio 11, IT-22100 Como, Italy*
[4]*Institute of Electronic Structures and Laser, Foundation for Research and Technology Hellas, P.O. Box 1527, 71110 Heraklion, Greece*
[5]*Materials Science and Technology Department, University of Crete, 71003 Heraklion, Greece*
[6]*Centre de Physique Theorique, Centre National de la Recherche Scientifique, Ecole Polytechnique, F-91128 Palaiseau, France**

(Received 7 January 2012; revised manuscript received 21 May 2012; published 5 September 2012)

We study cavitation dynamics when focusing ring-shaped femtosecond laser beams in water. This focusing geometry reduces detrimental nonlinear beam distortions and enhances energy deposition within the medium, localized at the focal spot. We observe remarkable postcollapse dynamics of elongated cavitation bubbles with high-speed ejection of microbubbles out of the laser focal region. Bubbles are ejected along the laser axis in both directions (away and towards the laser). The initial shape of the cavitation bubble is also seen to either enhance or completely suppress jet formation during collapse. In the absence of jetting, microbubble ejection occurs orthogonal to the laser propagation axis.

DOI: 10.1103/PhysRevE.86.036304 PACS number(s): 47.55.dp, 43.25.Yw, 47.55.dd, 52.50.Jm

I. INTRODUCTION

Cavitation is the process by which a liquid under an external force ruptures violently, leaving behind a void or bubble that subsequently implodes under the action of the external fluid pressure. Cavitation originally attracted interest in relation to the damage it can induce on ship propellers but it has since been discovered in a wide range of settings with important applications, for example, in chemical engineering, biomedical sciences, industrial cleaning, internal combustion engine efficiency, and interface science (see, e.g., [1–3] and references therein). Cavitation may be induced by mechanical forces (such as the aforementioned ship propeller or even a snapping shrimp claw [4]), by acoustic waves [3,5], or by tightly focused laser pulses [3]. In the following we will consider this last case, in which intense laser pulses are used to induce not only the liquid breakdown and hence the bubble formation but also the successive bubble cavitation dynamics.

Laser pulses may be used as an effective means to deposit large amounts of energy in very small volumes. The high light intensities at the focal spot ionize the medium and thus generate a highly localized plasma. The heated plasma expands violently, producing a shock wave that has been measured to have pressures from MPa up to TPa levels [6–8,10]. This rapid expansion in the surrounding medium leads to the formation of one or more bubbles whose evolution may be studied in a controlled environment. Laser-pulse induced cavitation has been used for a variety of applications. For example the emitted pressure shock wave can be refocused [8–10] or used for propulsion [11], luminescence similar to widely studied sonoluminescence has been observed [12,13], the bubbles themselves may be used for cell surgery under high numerical aperture focusing conditions [14–16], and the interaction (fusion, repulsion, jetting) of bubbles can be controlled for fundamental studies involving the interaction of the two-phase (air-liquid) interface with gravity [3,17].

An important feature of laser-pulse induced cavitation is the possibility to precisely tailor the shape of the bubble. Usually, long nanosecond pulses are used for inducing cavitation in liquids [3]. Such pulses generate bubbles with very high sphericity, a condition that is often required to observe the desired effects, e.g., cavitation-induced luminescence, or for comparison with hydrodynamic models. Spatial beam shaping has also been employed for generating elongated, multiple, or even arbitrarily shaped bubbles [18–21].

A further important phenomenon associated to cavitation is the formation of jets within the cavitating bubble, i.e., an intrusion of the vapor-liquid interface at one of the bubble walls towards the center of the bubble. These jets are of importance beyond fundamental studies; for example they may be used to increase biological cell permeability for drug injection [22,23]. The basic principles of jet formation are fairly well understood also for elongated bubbles (see, e.g., [6,18,24]): the collapse of aspherical bubbles starts at the parts of the bubble wall exhibiting the strongest curvature. Symmetrically counterpropagating jets or asymmetric jets can both be formed, depending on the initial bubble conditions. Recently it has been shown that the jet formation within large ($\gtrsim$1-mm diameter) spherical bubbles induced by nanosecond laser pulses is a direct consequence of gravitational forces acting on the bubble [17] and numerical simulations show that the jet direction can be controlled by using conically shaped bubbles [21].

In this work we investigate the cavitation dynamics of elongated bubbles induced by high-intensity, femtosecond laser pulses that are spatially shaped into a ring and then tightly focused into a water sample. Such a configuration achieves much tighter focusing conditions with respect to the axicon-focusing used in, e.g., Ref. [19]. At low input energies and/or small input focusing angles, we indeed observe cavitation dynamics similar to those reported in Ref. [19],

*d.faccio@hw.ac.uk

i.e., the formation of an elongated bubble that then contracts and disappears. However, at high ($\gtrsim$10–30 deg) focusing angles and relatively high input energies ($\gtrsim$10 μJ), that are therefore some one to two orders of magnitude higher than those used in previous studies, we observe a new cavitation regime characterized by rather remarkable bubble dynamics. The elongated bubble first expands violently along the minor axis, i.e., along the direction transverse to the laser-pulse propagation direction, and then suffers an equally violent contraction along the major axis. The cavitating bubble walls collide and break up into separate clusters of submicron sized bubbles. These clusters are ejected at high velocity away from the laser interaction region and reach large distances, of the order of 1 cm or more from the generating region. Interestingly, we observe that the microbubble clusters are always simultaneously ejected in both opposite directions along the laser propagation axis. Depending on the symmetry of the initial bubble, we may switch from ejection in the forward and backward direction to ejection in the transverse direction.

The ring-shaped focusing of femtosecond laser pulses therefore gives access to a wholly new range of bubble dynamics in liquids.

II. EXPERIMENTS

The experimental layout is shown in Fig. 1. The input beam from a 1-kHz repetition rate, 120-fs pulse duration, amplified Ti-Sapph laser is directed through a hole in a mirror onto a *W* axicon [25,26], i.e., a reflective element that transforms the input Gaussian beam into a ring. A first lens (lens 1) is used to control the thickness of this ring. The retroreflected ring is then directed by the first mirror onto lens 2 that focuses the ring into a cuvette filled with water. This ring-shaped focusing condition creates a Bessel-shaped beam in the focus. By changing the focal distance, f_2, of the focusing lens we

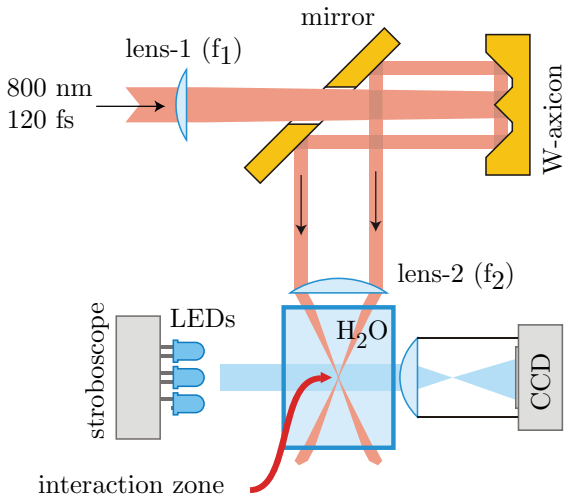

FIG. 1. (Color online) Experimental layout. The input Gaussian beam is transformed into a ring-shaped beam in reflection from the *W* axicon. The ring is focused into a cuvette filled with water and the laser-pulse induced cavitation bubble is monitored using a stroboscopic LED that illuminates the bubble whose image is magnified and collected on a CCD camera.

can change the angle of the Bessel beam $\theta = \arctan(R/f_2)$, where $R = 15$ mm is the radius of the ring. Such a focusing condition leads to complete suppression of distortion from nonlinear Kerr effects on the laser beam itself [27]. Indeed, at the intensities reached in our experiments, $\gtrsim 10^{13}$ W/cm^2, nonlinear propagation in the water medium would strongly modify an input Gaussian-shaped beam, leading to detrimental effects such as beam filamentation, white light generation, beam breakup, and clamping of the intensity to a maximum value of $\lesssim 10^{13}$ W/cm^2 [28]. Conversely, when using a ring-focusing geometry, the laser beam propagates at all times with low intensities, i.e., in the linear regime, with the sole exception of the very central core region formed by the central intense peak in the Bessel beam at the lens focus. The distance over which nonlinear Kerr effects accumulate on the pulse is limited to $L = D/\sin\theta$, where D is the diameter of the central Bessel peak (e.g., measured between the first two zeros) and is of the order of only several microns in our experiments (to be compared with typical Kerr nonlinear length, of the order of $\sim$100 μm). This effectively leads to a complete suppression of usual nonlinear effects and indeed no beam transformation or white light generation was observed in the range of energies used in our experiments.

The suppression of nonlinear propagation effects therefore guarantees a high beam quality at the lens focus. Moreover, the tight ring-beam focusing condition increases the maximum achievable intensity in the focal region. Indeed, the high intensities at the focal plane create a dense plasma through multiphoton absorption and tunneling ionization that depletes the pump laser-pulse energy. However, by increasing the input angle it is possible to replenish the energy fast enough to overcome these losses, thus enabling higher pulse peak intensities and, most importantly, higher plasma densities [27].

Figure 2 shows a photograph of the 2-cm-long water cuvette taken during a typical experiment. In this specific case we are focusing with a $\theta = 16.9$-deg-angle (in air) ring and 50-μJ input energy. The focal point of the laser beam is indicated with *F* and is $\sim$300 μm long. We include a video (from which Fig. 2 is extracted [29]) that shows the water cuvette, as seen by eye, with the transition from the usual cavitation regime to the microbubble ejection regime, as the laser input energy is slowly increased from 0 to 100 μJ. A stream of microbubbles can be seen along the laser propagation axis (the laser beam

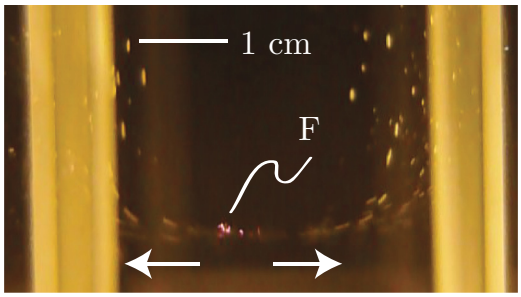

FIG. 2. (Color online) Photograph of the water-filled cuvette. A central bright spot indicates the laser focus, *F* (the laser beam is propagating from left to right). Bubbles are seen to be ejected over $\sim$1-cm distances along the laser beam propagation axis, in both the forward and backward directions.

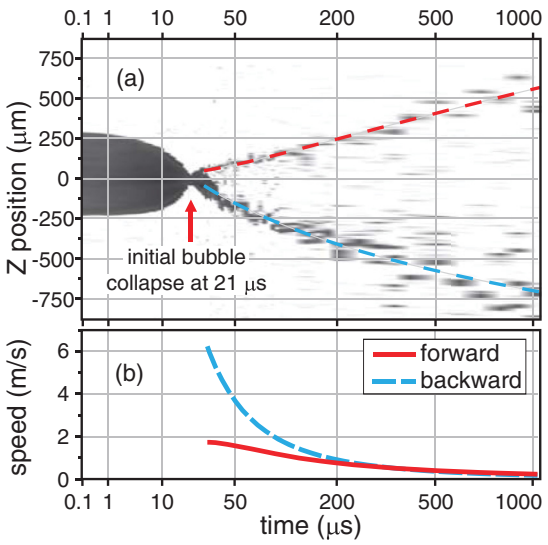

FIG. 3. (Color online) Evolution of the bubble position. Time zero corresponds to the instant in which the laser pulse is focused in the medium. (a) The dark region between time 0 and 21 μs, which is the main cavitating bubble that shrinks and then, after a slight rebound, breaks up into two clusters of microbubbles whose trajectories are highlighted by dashed lines. (b) The microbubble average ejection velocity, as given by the gradient of the bubble positions shown in (a).

propagates from left to right). Remarkably, these micron and submicron sized bubbles are ejected in a collimated stream directed in both the forward and backward directions with average velocities of a few m/s close to the laser focus. This initial velocity gives the microbubbles sufficient momentum to propagate horizontally over distances $\gtrsim$1 cm before slowing down and then rising vertically towards the water surface. As a first test we decreased the laser repetition rate down to 1 Hz in order to verify that the origin of the bubbles is truly due to the *postcollapse* stage of cavitating bubbles generated at the laser focus, as opposed to water boiling through high repetition-rate heat deposition. Indeed, even at 1 Hz, exactly the same dynamics were observed [29].

We can now analyze in more detail the main finding reported in this work, i.e., the microbubble ejection that occurs after the cavitating bubble has collapsed. Figure 3(a) shows the temporal evolution of the bubble longitudinal z position. The dark region that is seen to shrink for times up to 21 μs (indicated with an arrow in Fig. 3) is the main cavitating bubble. A slight rebound can be observed around 30 μs followed by a breakup into two sets of microbubble clusters which are ejected forward (positive z) and backward (negative z) with respect to the laser-pulse propagation direction. The gradient of the dashed lines (that highlight the average position versus time of the microbubble clusters) gives us the cluster average velocity, reported in Fig. 3(b), where we plot the absolute value of the velocities of the forward (solid line) and backward (dashed line) propagating bubbles. The backward bubbles appear to be ejected with the highest velocities, of the order of several m/s. The bubbles are seen to then slow down due to the effect of viscosity, reaching a velocity of $\sim$10 cm/s at a distance of several mm from the laser focus before finally reaching a halt at a distance of 1–2 cm from the laser focus and rising to the water cell surface (see Fig. 2).

In order to investigate the origin of the observed postcollapse dynamics of the cavitating bubbles and obtain more detailed information regarding the origin of the microbubble ejection, we performed detailed measurements of the *precollapse* stage by enlarging and imaging the laser focus region onto a CCD camera. Successive images of the cavitating bubble were captured using a stroboscopic LED light source (pulse duration $\sim$250 ns), synchronized with the laser that allowed 1-μs resolution. Examples of these measurements obtained with 38-μJ input energy and a focusing angle of $\theta = 26$ deg (in air) are shown in Fig. 4. The peak intensity of the laser pulse calculated assuming focusing in vacuum is $\sim 10^{15}$ W/cm^2 while a more reasonable evaluation based on a model that accounts for the nonlinear losses (energy deposition in the medium via multiphoton ionization processes) that occur at the focus predicts a maximum intensity of 4×10^{13} W/cm^2 in the medium [27]. Two different regimes were discovered depending on the cavitation bubble axial symmetry: a slight misalignment of the W axicon (obtained by tilting it with respect to the incoming laser beam axis) allows us to vary the energy distribution along the propagation z direction and thus influence the symmetry of the cavitation bubble, rendering it either very symmetric along the z direction or slightly asymmetric. Depending on this symmetry, very different behaviors were observed. Figure 4(a) shows the bubble evolution for a slightly asymmetric initial bubble and 38-μJ input energy: a few sample frames are shown from the full movie [29]. The bubble initially expands along the transverse x-y plane and reaches a maximum radius of $\sim$200 μm that is determined by the initial overpressure within the bubble [30]. The bubble then starts to collapse along the horizontal direction. As the two side walls move towards each other, a jet starts to form at $\sim$12 μs and is clearly visible at 17 μs. The jet extends inside the collapsing bubble and encounters the opposite wall with speeds up to 40–50 m/s. This is followed by a breakup of the whole cavitation bubble at $\sim$25 μs. The jet is directed along the horizontal direction and is therefore clearly not determined by gravitational forces as these act on the vertical direction [17]. Moreover, these jets cannot be assimilated to directionally controlled jets observed in the presence of elastic or rigid boundaries [24,31] as no such boundaries are present here. Rather, the observation of the jet depends on the initial geometrical shape of the cavitating bubble, which is solely induced by the laser pulse. In the present case, the right hand side wall of the bubble shows a clear imploding conical front likely to be induced by a Richtmier-Meshkov [32] or Rayleigh-Taylor [33] instability. The characteristics of the jet will depend on the cone angle, collapse velocity, and density step across the bubble front, as seen in numerical simulations involving conically shaped bubbles [21].

The successive bubble breakup is characterized by the formation of two clusters of μm-sized bubbles that propagate in opposite directions along the horizontal z axis with initial speeds of a few m/s. These form two streams of microbubbles moving in opposite directions and collimated along the laser propagation axis, as shown in Fig. 2.

Figure 4(b) shows the evolution for a symmetric initial cavitation bubble and the same 38-μJ input energy [29].

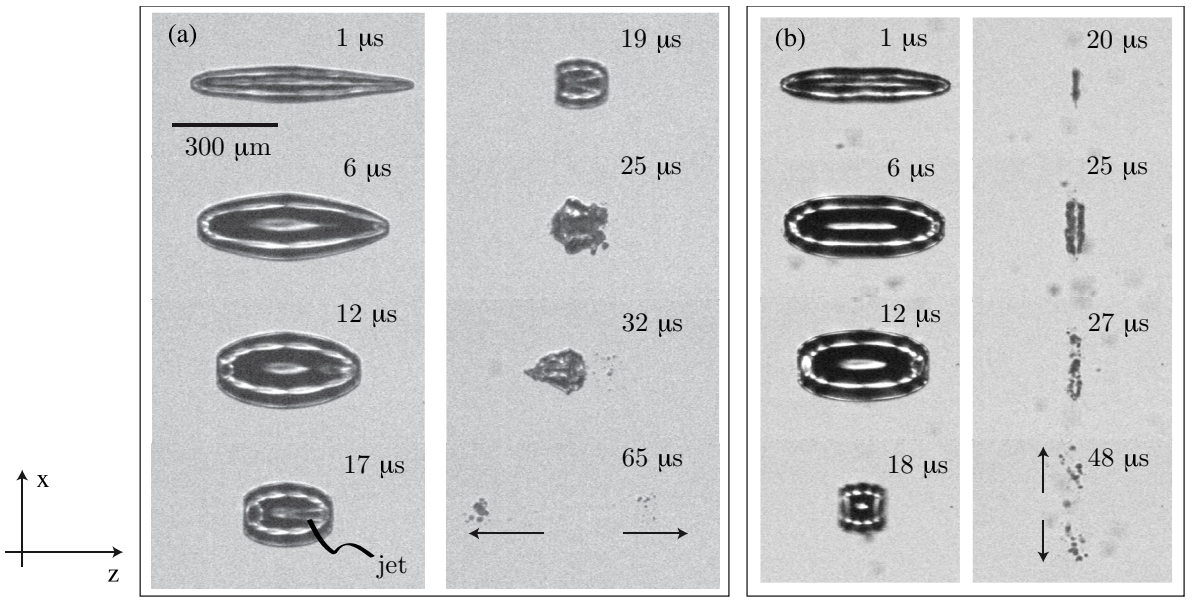

FIG. 4. Measured bubble evolution (a) for a slightly asymmetric initial bubble and (b) for a symmetric bubble. Arrows indicate the bubble cluster ejection directions in the two cases. The times in each figure indicate the time lapsed after the laser-pulse passage, defined to be time zero.

The initial dynamics are similar, with a strong expansion in the transverse x-y plane. However, as the side walls start to collapse along the z direction a jet is no longer formed and the two walls remain parallel to each other while moving at speeds of ~40 m/s. When the two walls encounter each other, they suffer an initial rebound (25 μs) and then break up into clusters of μm-sized bubbles that are now ejected in the transverse x-y plane (48 μs).

In Figs. 5(a) and 5(b) we show the cavitation bubble x-z dimensions (Dx, Dz) and bubble wall velocities (vx, vz) versus time for both the asymmetric (squares) and symmetric (circles) initial conditions described above. In Fig. 5(b) positive velocities indicate expansion and negative velocities indicate contraction. We note that although in the two cases we had different initial Dz the evolution of Dx remains practically identical. This is due to the fact that the bubble expansion, that occurs predominantly in the transverse x-y plane, is determined largely by the initial overpressure and not by the geometrical shape of the bubble.

From the images of the cavitation bubble we may also derive the bubble volume (assuming azimuthal symmetry), as reported in Fig. 5(c), for the two cases discussed above and also for a symmetric bubble with 100-μJ energy. The cavitating bubbles at 38-μJ input energy have very similar volumes with only a slight difference due to the initial difference in Dz [see Fig. 5(a)]. The bubble at 100 μJ had identical Dz to the 38-μJ case but exhibits a much stronger expansion in the x-y plane (hence the larger volume), thus indicating that higher input energies lead to higher initial overpressures. This clearly indicates that the cavitation bubble overpressure is directly related to the energy deposited in the medium through ionization by the input laser pulse. This increase in bubble volume with input laser energy is also in agreement with other measurements in this sense [34,35].

We briefly return to the jet structure observed with asymmetric bubbles. This structure is observed at all energies and appears to be a common feature of all cavitation regimes

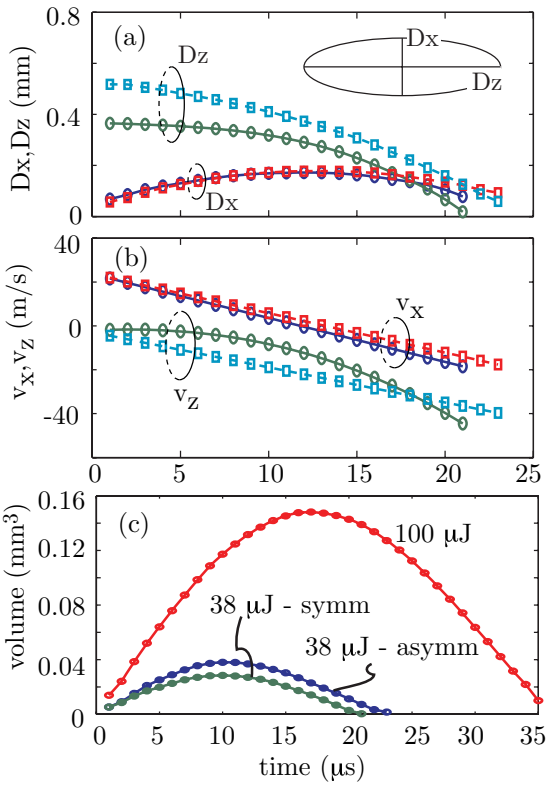

FIG. 5. (Color online) (a) Time evolution of the bubble longitudinal (Dz) and transverse (Dx) dimensions. (b and c) Evolution (b) of the bubble wall velocities and (c) of the bubble volume for input pulse energies indicated in the figure.

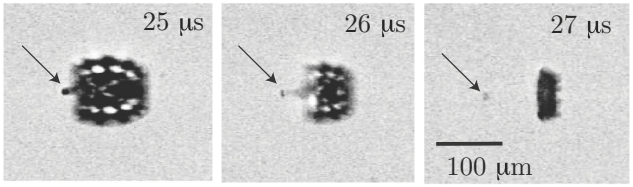

FIG. 6. Details of jet evolution at the moment of impact with the colliding opposite bubble wall. Input energy is 100 μJ. The arrow indicates the position of the jet tip.

investigated with our setup as long as the bubble exhibits some initial asymmetry. In Fig. 6 we show the details of the jet structure measured with 100-μJ input energy. The jet is clearly seen to pierce the opposite bubble wall and extends well beyond into the surrounding liquid. The last frame at 27 μs shows a remnant of the jet that appears to be completely detached from the rest of the cavitation bubble. The emission direction of the ejected bubble clusters appears to be clearly linked to the presence of this jet.

We may at this stage speculate that the jet, moving at speeds larger than 50 m/s inside the bubble, creates a strong radial force that will generate a vortex ring in the postcollapse stage of the cavitating bubble [36]. Under usual operating conditions, the self-propelling vortex ring is generated by the jet and leads to expulsion of microbubbles in the transverse direction. In our case we observe a modification of these dynamics whereby the vortex ring (generated around $t \sim 25$ μs in Fig. 4) does not continue expanding but rather remains stationary or rebounds and thus induces a flow orthogonal to the ring itself, i.e., in both opposite directions along the jet axis. This flow in turn leads to the opposing microbubble streams along the laser axis, as observed in our experiments. Conversely, when the jet is absent, the colliding walls remain parallel to each other and they experience a force that is directed mainly along the z axis but will have a radial component at the external borders. This may still lead to the formation of a vortex ring and to the observed microbubble ejection in the x-y plane, albeit in the absence of any evidence of jetting.

III. CONCLUSIONS

In conclusion, these measurements show that the long-sought-after goal of increasing the violence of cavitating bubble collapse is possible, thus yielding more extreme conditions inside the bubble [37]. In particular, we observe a final collapse stage that is dominated by the cavitating bubble breakup and the ejection at high speeds of microbubble clusters. We underline that the dynamics observed are not linked in any way to the repetition rate of the laser source. Indeed, exactly the same bubble ejection dynamics were observed at all repetition rates down to 1 Hz and even in single shot measurements. In the single shot regime, individual microbubbles are ejected to large distances. At high laser repetition rates these merge into what appear as two collimated streams directed in opposite directions along the laser-pulse propagation axis.

The results shown were obtained in water, but other liquids, e.g., methanol and ethanol, exhibit a similar behavior. Some of the main mechanisms at play in the jet formation and bubble dynamics were evidenced by our measurements, from which we proposed the scenario outlined in the description of Fig. 4. Refinement of this scenario and uncovering the full dynamics will require further study and numerical investigation such as those shown, e.g., in Refs. [3,21,32,38]. Yet the phenomenon of microbubble ejection holds promise for a wide range of applications, such as cell surgery and drug injection [22,23], surface cleaning [39], and bubble control of microfluidic systems [40,41].

ACKNOWLEDGMENT

The authors acknowledge financial support from EU-FP7, project LASERLAB-EUROPE access, Grant No. 228334.

[1] P. R. Gogate and A. M. Kabadi, Biochem. Eng. J. **44**, 60 (2009).
[2] F. Caupin and E. Herbert, C. R. Phys. **7**, 1000 (2006).
[3] W. Lauterborn and T. Kurz, Rep. Prog. Phys. **73**, 106501 (2010).
[4] M. Versluis, B. Schmitz, A. von der Heydt, and D. Lohse, Science **289**, 2114 (2000).
[5] M. P. Brenner, S. Hilgenfeldt, and D. Lohse, Rev. Mod. Phys. **74**, 425 (2002).
[6] A. Vogel, S. Busch, and U. Parlitz, J. Acoust. Soc. Am. **100**, 148 (1996)
[7] J. Noack, D. X. Hammer, G. D. Noojin, B. A. Rockwell, and A. Vogel, J. Appl. Phys. **83**, 7488 (1998).
[8] G. N. Sankin, Y. F. Zhou, and P. Zhong, J. Acoust. Soc. Am. **123**, 4071 (2008).
[9] S. Juodkazis, K. Nishimura, S. Tanaka, H. Misawa, E. G. Gamaly, B. Luther-Davies, L. Hallo, P. Nicolai, and V. T. Tikhonchuk, Phys. Rev. Lett. **96**, 166101 (2006).
[10] T. Pezeril, G. Saini, D. Veysset, S. Kooi, P. Fidkowski, R. Radovitzky, and K. A. Nelson, Phys. Rev. Lett. **106**, 214503 (2011).
[11] B. Han, Y- X. Pan, Y- L. Xue, J. Chen, Z- H. Shen, J. Lu, and X- W. Ni, Opt. Lasers Engin. **49**, 428 (2011).
[12] C.-D. Ohl, O. Lindau, and W. Lauterborn, Phys. Rev. Lett. **80**, 393 (1998).
[13] O. Baghdassarian, B. Tabbert, and G. A. Williams, Phys. Rev. Lett. **83**, 2437 (1999).
[14] V. Venugopalan, A. Guerra, K. Nahen, and A. Vogel, Phys. Rev. Lett. **88**, 078103 (2002).
[15] A. Vogel, N. Linz, S. Freidank, and G. Paltauf, Phys. Rev. Lett. **100**, 038102 (2008).
[16] A. Vogel, J. Noack, G. Hüttman, and G. Paltauf, Appl. Phys. B **81**, 1015 (2005).
[17] D. Obreschkow, M. Tinguely, N. Dorsaz, P. Kobel, A. de Bosset, and M. Farhat, Phys. Rev. Lett. **107**, 204501 (2011).
[18] R. P. Godwin, E. J. Chapyak, J. Noack, and A. Vogel, Proc. SPIE **3601**, 225 (1999).
[19] I. Toytman, D. Simanovski, and D. Palanker, Opt. Express **18**, 24688 (2010).
[20] K. Yang, Y. Zhou, Q. Ren, J. Yong Ye, and C. X. Deng, Appl. Phys. Lett. **95**, 051107 (2009).

[21] K. Y. Lim, P. A. Quinto-Su, E. Klaseboer, B. C. Khoo, V. Venugopalan, and C. D. Ohl, Phys. Rev. E. **81**, 016308 (2010).
[22] P. Prentice, Cuschieri, A. Dholakia, K. Prausnitz, and M. Campbell, Nat. Phys. **1**, 107 (2005).
[23] C.-D. Ohl, M. Arora, R. Ikink, N. de Jong, M. Versluis, M. Delius, and D. Lohse, Biophys. J. **91**, 4285 (2006).
[24] E. A. Brujan, K. Nahen, P. Schmidt, and A. Vogel, J. Fluid Mech. **433**, 251 (2001).
[25] R. M. Gilgenbach and L. D. Horton, Rev. Sci. Instrum. **55**, 503 (1984).
[26] M. Lei and A. Zumbusch, Opt. Lett. **35**, 4057 (2010).
[27] D. Faccio, E. Rubino, A. Lotti, A. Couairon, A. Dubietis, G. Tamosauskas, D. G. Papazoglou, and S. Tzortzakis, Phys. Rev. A **85**, 033829 (2012).
[28] A. Couairon and A. Mysyrowicz, Phys. Rep. **441**, 47 (2007).
[29] See Supplemental Material at http://link.aps.org/supplemental/10.1103/PhysRevE.86.036304 for a movie showing the water cuvette, as seen by eye, with the transition from the usual cavitation regime to the microbubble ejection regime; for a movie showing the bubble dynamics observed at low, 4-Hz, laser repetition rate; for a movie showing the detail of the cavitation bubble evolution for a slightly asymmetric initial bubble leading to microbubble emission along the laser propagation axis; for a movie showing the detail of the cavitation bubble evolution for a symmetric initial bubble leading to microbubble emission perpendicular to the laser propagation axis.
[30] K. Tsiglifis and N. A. Pelekasis, Phys. Fluids **19**, 072106 (2007).
[31] T. B. Benjamin and A. T. Ellis, Phil. Trans. R. Soc. Lond. A **260**, 221 (1966).
[32] E. E. Meshkov, Sov. Fluid Dyn. **4**, 101 (1969).
[33] D. H. Sharp, Physica D **12**, 3 (1984).
[34] S. R. Aglyamov, A. B. Karpiouk, F. Bourgeois, A. Ben-Yakar, and S. Y. Emelianov, Opt. Lett. **33**, 1357 (2008).
[35] D. Tiwari, Y. Bellouard, A. Dietzel, M. Ren, E. Rubingh, and E. Meinders, Appl. Phys. Express **3**, 127101 (2010).
[36] A. Vogel, W. Lauterborn, and R. Timm, J. Fluid Mech. **206**, 299 (1989).
[37] T. Kurz, D. Kröninger, R. Geisler, and W. Lauterborn, Phys. Rev. E **74**, 066307 (2006).
[38] K. Tsiglifis and N. A. Pelekasis, Phys. Fluids **17**, 102101 (2005).
[39] C.-D. Ohl, M. Arora, R. Dijkink, V. Janve, and D. Lohse, Appl. Phys. Lett. **89**, 074102 (2006).
[40] P. Marmottant and S. Hilgenfeldt, Proc. Nat. Acad. Sci. USA **101**, 9523 (2004).
[41] K. Zhang, A. Q. Jian, X. M. Zhang, Y. Wang, Zh. H. Li, and H. Y. Tamc, Lab Chip **11**, 1389 (2011).